J Sol-Gel Sci Technol (2016) 79:426–439
DOI 10.1007/s10971-015-3923-x

ORIGINAL PAPER : NANO- AND MACROPOROUS MATERIALS (AEROGELS, XEROGELS, CRYOGELS, ETC.)

Concentration-dependant selective removal of Cr(III), Pb(II) and Zn(II) from aqueous mixtures using 5-methyl-2-thiophenecarboxaldehyde Schiff base-immobilised SBA-15

Surendran Parambadath[1] · Aneesh Mathew[1] · Mary Jenisha Barnabas[1] · Su Yeon Kim[1] · Chang-Sik Ha[1]

Received: 29 July 2015 / Accepted: 20 November 2015 / Published online: 22 December 2015

Abstract 5-Methyl-2-thiophenecarboxaldehyde (MTC)-derived Schiff base was immobilised over SBA-15 (TS-SBA-15) via a two-step modification procedure. Initially, (3-aminopropyl)triethoxysilane (APTES) was heterogenised over SBA-15 (NH_2-SBA-15), and the Schiff base formation was followed by a reaction with MTC in hot methanol. X-ray diffraction and transmission electron microscopy showed that the SBA-15, NH_2-SBA-15 and TS-SBA-15 materials had mesoscopically ordered, hexagonal symmetry and well-defined morphologies. ^{29}Si magic-angle spinning nuclear magnetic resonance (MAS NMR) spectroscopy revealed a change in the silicon environment during modification. The N_2 sorption experiments showed that the material has a large surface area (623 m^2 g^{-1}), acceptable pore diameter (6.5 nm) and reasonable pore volume (1.23 cm^3 g^{-1}) to accommodate the guest molecules inside the pore channels. Organic functionalisation was determined successfully by Fourier transform infrared and ^{13}C cross-polarisation magic-angle spinning NMR spectroscopy. The optimal condition for the removal of Cr(III), Pb(II) and Zn(II) from water was explored by varying the parameters, such as pH, stirring time, initial concentration and amount of adsorbent. The results suggested that TS-SBA-15 can achieve the adsorption maximum within 6 h at pH 6.5. The adsorbent exhibited moderate-to-good adsorption ability towards the three metal ions under these experimental conditions. The selective adsorption performance of TS-SBA-15 from binary mixture was examined by keeping equal concentrations of metal ions in the mixture. TS-SBA-15 was more selective towards Cr(III) ions from both the binary and ternary mixtures at pH 6.5. The effect of the metal ion concentration over mole adsorption selectivity in the ternary mixture was examined by doubling the concentration of at least one metal ion in the mixture. The result was compared with the ternary mixture containing equal concentrations of metal ions. The reusability test showed that TS-SBA-15 can be recycled for at least six consecutive cycles without losing its adsorption ability.

Graphical Abstract

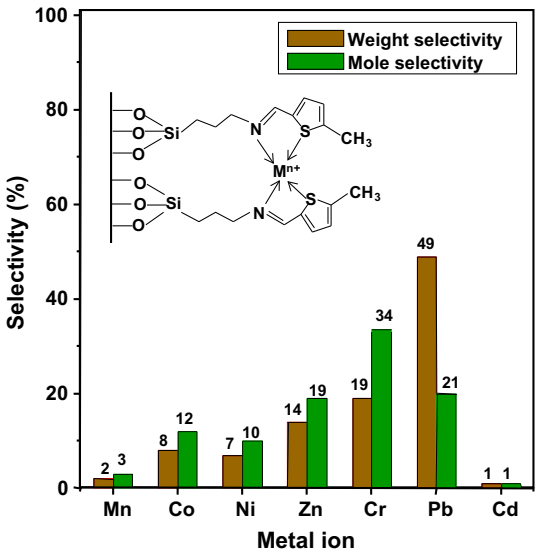

Electronic supplementary material The online version of this article (doi:10.1007/s10971-015-3923-x) contains supplementary material, which is available to authorized users.

✉ Chang-Sik Ha
csha@pusan.ac.kr

[1] Department of Polymer Science and Engineering, Pusan National University, Geumjeong-gu, Busan 609-735, Korea

Keywords SBA-15 · 5-Methyl-2-thiophenecarboxaldehyde · Schiff base · Metal adsorption

1 Introduction

Since the discovery of mesoporous silica M41S, which is prepared via sol–gel chemistry, mesoporous materials have attracted considerable attention because of their potential applications in catalysis, membrane filtration and separation technology and the adsorption of ions or organic compounds of large sizes [1–5]. These solids exhibit high specific surface areas, high crystallinity, high thermal stability and uniformity of the hexagonal cylindrical pores, narrow pore distribution and regulated pore diameter ranging from 15 to 100 Å. Moreover, the silica wall surface can be modified with organic groups to tailor their properties and achieve specific purposes. The organic functionalisation of these mesoporous inorganic materials has attracted considerable interest because of the appeal of combining a wide range of organic compound properties with the robust thermal and mechanical stabilities of inorganic solids. SBA-15 is one of the most popular mesoporous silica because of its large pore size, which allows easier accessibility to the inner surface of the material, indicating many applications [6]. Over the last few decades, huge effort has been made to modify the SBA-15 surface with a range of functional groups because the material is considered to have great potential for adsorption/separation applications [7]. Mineral processing and metal-finishing industries produce large amounts of waste effluent containing chromium, copper, nickel, cobalt, zinc, lead, cadmium and other harmful elements [8].

A wide variety of techniques can be used to remove heavy metals from water, such as ion exchange, reverse osmosis and nanofiltration, precipitation, coagulation/co-precipitation and adsorption [9–12]. The adsorption of heavy metals by functionalised mesoporous materials is a relatively recent and popular method owing to its simplicity and low cost. Therefore, increasing pressure from environmental authorities has forced the establishment of discharge limits, which in turn requires more effective decontamination and purification methods, such as the use of porous materials to remove metal ions from aqueous solution. For adsorption purposes, chelating agents should be immobilised on solid carriers. This type of adsorbent may potentially extract heavy metal ions from both acidic and basic media [13–16].

Schiff base compounds, which can be prepared easily by condensation between aldehydes and amines, are very efficient chelating agents. In addition, Schiff bases, which contain nitrogen, sulphur and oxygen donor atoms, tend to show high selectivity towards the complexation of heavy metal ions under optimal conditions. The ability of a material to chelate with metals is controlled in part by the number of available functional groups used for metal ion chelation [17, 18]. Previous studies suggested that the immobilisation of Schiff base ligands onto mesoporous solid supports led to the formation of materials, which are efficient adsorbents for heavy metal ions [19, 20]. Note that solid-phase extraction techniques have numerous advantages, such as flexibility, high preconcentration factors, high capture capacity, speed and simplicity, possibilities for field sampling and ease of automation [21]. To date, researchers have proposed different chelating ligand-immobilised materials for the removal of Cr(III), Zn(II) and Pb(II) from different sources of water [22–24]. In particular, heterogeneous 2-thiophenecarboxaldehyde Schiff has been used extensively by researchers to capture a wide spectrum of metal ions from aqueous sources under a range of pH conditions [25, 26]. Chemically bonded 2-thiophenecarboxaldhyde to silica gel surface through monoamine, ethylenediamine and diethylenetriamine was found to be highly efficient for adsorbing metal ions such as Ca(II), Fe(III), Co(II), Ni(II), Cu(II), Zn(II), Cd(II), Hg(II) and Pb(II) under various pH conditions [25] and was highly selective for Hg(II) ions. In another report, 2-thiophenecarboxaldhyde immobilized to mesoporous MCM-41 through monoamine was also found to be active for Pd(II) from water. Also the adsorption of Pd(II) was found to be independent on the presence of various co-existing ions in the adsorption medium [26]. It was observed that the previous researchers were mainly focused on the adsorption efficiency of 2-thiophenecarboxaldehyde Schiff base-modified heterogeneous systems, and the selectivity was not much concerned. Also it is important to consider the selective removal of Cr(III), Pb(II) and Zn(II) metal ions from water sources as a matter of environmental concern especially. The Schiff base complexes are highly active towards these metal ions under various pH conditions. In order to attain better selectivity for such metal ions, it is necessary to modify the 2-thiophenecarboxaldehyde Schiff without compromising the activity. Therefore, the presence of an electron donor, such as $-CH_3$, in the thiophene ring should increase the metal adsorption efficiency and selectivity of the Schiff base ligand.

Based on this background, this paper describes the immobilisation of 5-methyl-2-thiophenecarboxaldehyde on aminopropyl-functionalised SBA-15 through Schiff base formation, which provides a simple and potential electron donor ligand for accommodating metal ions from aqueous mixtures. Moreover, the post-synthesis method allows a high loading and dispersion of functional molecules per gram to capture larger amounts of metal ions from various aqueous mixtures using much smaller amounts of support material. This study examined the effects of various

parameters, such as pH, stirring time, initial concentration and amount of adsorbent on adsorption. The adsorption performance of the obtained material was investigated from individual, binary and ternary metal solutions with or without varying the metal ion concentration, because the dependence of selectivity on the concentration of metal ion in a mixture was the main concern in this study.

2 Experimental

2.1 Reagents and materials

Tetraethylorthosilicate (TEOS), Pluronic P123, (M_w = 5800, $EO_{20}PO_{70}EO_{20}$), (3-aminopropyl)triethoxysilane (APTES), 5-methyl-2-thiophenecarboxaldehyde (MTC), chromium(III)nitrate nonahydrate [$Cr(NO_3)_3{\cdot}9H_2O$], zinc (II)nitrate hexahydrate [$Zn(NO_3)_2{\cdot}6H_2O$], lead(II)nitrate [$Pb(NO_3)_2$] and anhydrous toluene were purchased from Sigma-Aldrich (Germany). All chemicals were used as received.

2.2 Synthesis of SBA-15

Siliceous SBA-15 was synthesised via a sol–gel reaction using the procedure reported elsewhere [27] with the following initial molar compositions, 0.043 TEOS:4.4 g P123 Mavg = 5800 [EO_{20}-PO_{70}-EO_{20}]:8.33 H_2O:0.24 HCl. Typically, 4.4 g of triblock co-polymer was dispersed in 30.0 g distilled water and stirred for 1.5 h. To the resulting solution, 120.0 g of 2 M HCl was added with stirring, and the stirring was continued for 2 h. Finally, 9.0 g of TEOS was added drop-wise, and the mixture was maintained at 35 °C for 24 h without stirring. The resulting heterogeneous mixture was submitted to a hydrothermal treatment at 100 °C for 48 h under static conditions before recovering the solid material. The crystallised product was filtered, washed with distilled water and dried in air for 12 h, and in an oven at 70 °C for 12 h. Calcination was carried out at 450 °C for 8 h in air to remove the template completely. The structure of the SBA-15 was confirmed by small-angle X-ray scattering (SAXS) and N_2-sorption analysis.

2.3 Preparation of NH_2-SBA-15

The APTES-functionalised SBA-15 (NH_2-SBA-15) was prepared using the method described elsewhere [7]. APTES (1.0 g, 4.5 mmol) was added drop-wise to vacuum-dried SBA-15 (1.0 g) dispersed in toluene (50.0 ml) with vigorous stirring in a nitrogen atmosphere. The mixture was then heated under reflux for 24 h. The final product was filtered, washed several times with toluene, dichloromethane and ethanol and dried at 60 °C in vacuum for 12 h. The product is called NH_2-SBA-15 (Scheme 1).

2.4 Preparation of TS-SBA-15

MTC Schiff base formation was carried out using the methodology reported in the literature [28]. NH_2-SBA-15 (1.0 g) was dispersed in 100.0 ml dry methanol, followed by the addition of a solution of MTC (0.58 g, 5.0 mmol) in dry methanol (10.0 ml) drop-wise under a nitrogen atmosphere. The mixture was homogenised by stirring for 1 h at room temperature under a nitrogen atmosphere. The entire mixture was placed in an oil bath and heated to 65 °C for 12 h with stirring. The product was filtered, washed several times with methanol and dried at 60 °C in vacuum for 12 h. The product was called TS-SBA-15 (Scheme 1).

2.5 Competitive adsorption from a multiple metal ion solution

Competitive adsorption by TS-SBA-15 from a solution containing 1 mM each of Mn(II), Co(II), Ni(II), Cr(III), Zn(II), Pb(II) and Cd(II) ions at pH 6 was conducted to select the metal ions for the detailed adsorption study. The solution pH was adjusted by adding a 0.1 M NaOH solution. In total, 0.01 g of TS-SBA-15 was added to 10 ml of the above solution and shaken for 24 h to establish the adsorption equilibrium. The mixture was filtered, and the amount of various metals adsorbed was measured by inductively coupled plasma atomic emission spectroscopy (ICP-AES).

2.6 Adsorption from individual metal ion solutions

A solution containing Cr(III)/Pb(II)/Zn(II) ions was prepared by dissolving a known amount of the corresponding nitrate salt in distilled water. The concentration of metal ions ranged from 1 to 5 mM, and the adsorption experiments were conducted by suspending 0.01 g of TS-SBA-15 in 10.0 ml of an aqueous metal ion solution at pH 6.5. The effect of pH on the metal ion uptake was examined by performing equilibrium sorption experiments by varying the solution pH from 3.0 to 6.5. The solution pH was adjusted by adding either 0.1 M HNO_3 or 0.1 M NaOH. TS-SBA-15 (0.01 g) was added to the aqueous metal solution (10.0 ml, 1.0–5.0 mM) and shaken for the desired time at 25 °C. The adsorbent was filtered out through a polypropylene microfilter, and the amount of Cr(III)/Pb(II)/Zn(II) adsorbed by TS-SBA-15 was measured by ICP-AES. The amounts of Cr(III)/Pb(II)/Zn(II) adsorbed were calculated from the difference between the initial (C_o) and equilibrium (C_e) concentrations in the supernatant after centrifugation. The adsorption percentage [adsorption (%) = $(C_o - C_e)/C_o \times 100$] was derived from the difference between C_o and C_e.

2.7 Adsorption from binary and ternary metal ion solutions

The competitive metal adsorption efficiency of TS-SBA-15 was assessed using binary and ternary metal ion solutions containing 1.0 mmol of Cr(III), Pb(II) and Zn(II) nitrate salts in distilled water. The effects of the concentration of the component metal ions in a mixture on the adsorption selectivity were examined using three ternary solutions for adsorption, in which the concentration of at least one component was doubled. The pH of the solution was adjusted to 6.5 using a 0.1 M NaOH solution. TS-SBA-15 (0.01 g) was suspended in the binary or ternary solution (10.0 ml) and shaken mechanically at 25 °C for 6 h. The mixture was filtered out, and the amount of various metals adsorbed was determined by ICP-AES analysis.

2.8 Characterisation

Small-angle X-ray scattering (SAXS) was performed at the Pohang Accelerator Laboratory (PLA), POSTECH, Korea, with Co Kα ($\lambda = 1.608$ Å) radiation. Scanning electron microscopy (SEM, JEOL 6400) was conducted at an acceleration voltage of 20 kV. Transmission electron microscopy (TEM, JEOL 2010) was performed at an accelerating voltage of 200 kV. The N_2 adsorption–desorption isotherms were measured using a Nova 4000e surface area and pore size analyser. The samples were degassed at 120 °C for 12 h before the measurements. The Brunauer–Emmet–Teller (BET) method was used to calculate the specific surface area. The pore size distribution curve was obtained from an analysis of the adsorption branch using the Barrett–Joyner–Halenda (BJH) method. Fourier transform infrared (FTIR, JASCO FTIR 4100) spectroscopy was performed using KBr pellets in the frequency range, 4000–400 cm^{-1}. Thermogravimetric analysis (TGA, PerkinElmer Pyris Diamond) was carried out at a heating rate of 10 °C min^{-1} in air. ^{13}C CP and ^{29}Si magic-angle spinning (MAS) NMR (Bruker DSX 400) spectroscopy was performed with a 4-mm zirconia rotor spinning at 6 kHz (resonance frequencies of 79.5 and 100.6 MHz for ^{29}Si and ^{13}C CP-MAS NMR, respectively; 90° pulse width of 5 ms, contact time of 2 ms, recycle delay of 3 s for both ^{29}Si MAS and ^{13}C CP-MAS NMR). Quantitative determination of the metal ion content was performed by ICP-AES (ACTIVA, JYHORIVA, Japan).

3 Results and discussion

3.1 SAXS analysis

The SAXS patterns of the (a) SBA-15 shown in Fig. 1 exhibited a well-resolved diffraction peak at q (scattering vector) values = 0.6 nm^{-1} and two weak peaks at 1.09 and 1.29 nm^{-1} due to (100), (110) and (200) reflections, respectively, indicating the existence of a hexagonal mesophase within the samples. The same trend was observed on the SAXS patterns of the (b) NH_2-SBA-15 and (c) TS-SBA-15 samples compared to the SBA-15 support [29]. The intensity of the diffraction peaks of SBA-15 was higher than that of NH_2-SBA-15 and TS-SBA-15. This suggests that the former possessed a more ordered mesophase than the latter. The position of the (100), (110) and (200) reflections in the NH_2-SBA-15 and TS-SBA-15 samples was shifted slightly to a high q value compared with the same of the SBA-15, indicating small pore contraction due to functionalisation and further modification. The q values of the (100), (110) and (200) reflections were 0.65, 1.13 and 1.31 nm^{-1} for NH_2-SBA-15 and 0.66, 1.15 and 1.35 nm^{-1} for TS-SBA-15, respectively. The sharpness of the reflections indicated the quality of the materials. On the other hand, the framework of the samples was not changed and the porous channels remained in a hexagonal array, even after chemical modification [30]. The TS-SBA-15 sample had lower reflection intensity than SBA-15 because the pore channels were filled with a MTC Schiff base.

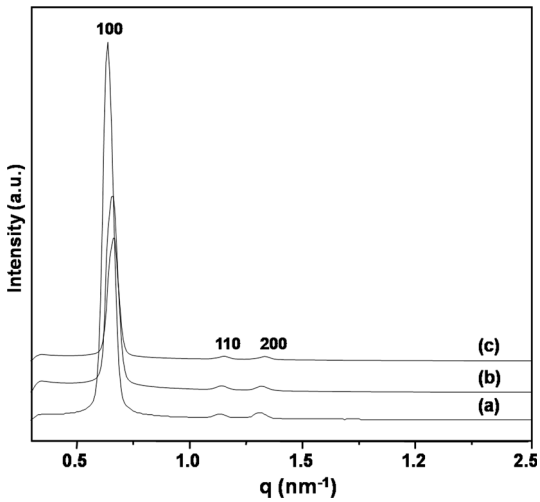

Fig. 1 SAXS patterns of (*a*) SBA-15, (*b*) NH_2-SBA-15 and (*c*) TS-SBA-15

3.2 SEM and TEM analysis

The morphology and texture of mesoporous silica are extremely important and can vary with the synthesis parameters. The external morphology of the (a) SBA-15, (b) NH_2-SBA-15 and (c) TS-SBA-15 was characterised by SEM, which can be observed from Fig. S1. All the samples showed rope-like shapes with a typical diameter and length of the rope segment of approximately 0.35 and 1 μm,

respectively [31]. The morphology was intact even after aminopropyl functionalisation and subsequent Schiff base modification. The surface morphology of (a) SBA-15, (b) NH_2-SBA-15 and (c) TS-SBA-15 was observed by TEM (Fig. S2). The TEM images of SBA-15 and modified SBA-15 revealed a honeycomb-like array (Fig. S2a, c and e) and strip-like patterns (Fig. S2b, d and f); the black strips represent the silica walls, whereas the white ones are associated with the hollow mesopores [27, 32]. Regular and extended pore periodicity along with an ordered hexagonal pore structure was observed. After functionalisation with aminopropyl and MTC Schiff base, the textural properties, such as the particle size, morphology, long-range pore order and hexagonal pore structure, of the SBA-15 material were not altered, indicating the persistence of uniform ordered mesoporous materials.

3.3 Nitrogen adsorption/desorption isotherms

The N_2 sorption isotherms were measured for the pure support and immobilised molecules, representing a comparison of the sorption isotherms and textural characteristics of pure and immobilised molecules. Figure S3A and B presents the low-temperature nitrogen adsorption–desorption isotherms and pore size distributions of the 2D hexagonal (*p6mm*) (a) SBA-15, (b) NH_2-SBA-15 and (c) TS-SBA-15, respectively. All the isotherms displayed type IV patterns with steep capillary condensation/evaporation steps in the range, $P/P_o = 0.44$–0.83 and obvious H1 hysteresis loops characteristics of mesoporous materials with cylindrical pores according to the IUPAC classification. The typical regions could be discerned in the isotherm of SBA-15, which clearly indicates the formation of a SBA-15 material [27]. In addition, SBA-15 exhibited a sharp capillary condensation step in the adsorption and desorption curve at partial relative pressures P/P_o of 0.62–0.83. Similarly, Type IV curves with H1 hysteresis loops were also obtained in the NH_2-SBA-15 and TS-SBA-15 samples with hysteresis loops shifting gradually to lower relative pressures and the volumes of nitrogen adsorbed decreasing after functionalisation. The phenomenon is typical of pore-plugging, suggesting that the partial channels are filled with guest species [33]. The BET surface areas of SBA-15, NH_2-SBA-15 and TS-SBA-15 were 623, 485 and 396 $m^2\ g^{-1}$, the pore volumes were 1.23, 0.67 and 0.41 $cm^3\ g^{-1}$, and the pore diameters were 6.5, 5.8 and 5.5 nm, respectively (Table 1). These values indicated the expected decrease in surface area, pore diameter and pore volume as a result of the modifications. The decrease in surface area during the surface modification process is responsible for the decrease in pore volume and pore diameter. The specific surface area decreased from 623 to 485 $m^2\ g^{-1}$ ($\sim$22 % decrease), while functionalisation with (3-aminopropyl)triethoxysilane on calcined SBA-15 clearly points out the anchoring of a considerable amount of tethering molecule, which aims to passivate the hydroxyl groups inside the pores of the calcined silica support [34]. A further but small decrease in surface area for TS-SBA-15 (396 $m^2\ g^{-1}$) was attributed to ligand immobilisation over NH_2-SBA-15, which indicated that the undisturbed silica surface remained even after functionalisation and ligand immobilisation. SBA-15 shows a narrow pore size distribution with a mean value of 6.5 nm. The modified materials (NH_2-SBA-15 and TS-SBA-15) also showed partially narrow and lower pore size distributions, which suggest that the Schiff base molecule is distributed uniformly all over the SBA-15 channel surface. The insertion of organic molecules inside the channels of the mesoporous materials was further evidenced from the measurements of the pore volume of the synthesised materials. The pore volume decreased considerably after the functionalisation of propylamine and its conversion to Schiff base to pure SBA-15, indicating the progress of anchoring of the organic moieties inside the channels [35]. But only a small amount of decrease in pore volume during the conversion of NH_2-SBA-15 to TS-SBA-15 was observed, which is further supported from the pore diameter values of these materials that also have not been changed considerably during the Schiff base formation.

3.4 FTIR spectral studies

Figure 2 shows the FTIR spectra of (a) NH_2-SBA-15 and (b) TS-SBA-15. The entire spectra showed a broad and strong vibrational band between 3700 and 3200 cm^{-1}, which can be assigned to the O–H stretching vibration of adsorbed water molecules and hydrogen bonded surface silanol in the SBA-15 matrix [27, 35]. The small band due to the Si–OH bond stretching vibration of the silanol groups was observed at 970 cm^{-1}. This smaller amount of silanol groups indicates the utilisation of a major portion of the silanol groups for functionalising the APTES on the

Table 1 Physico-chemical properties from N_2-sorption analysis of SBA-15 materials before and after modifications

Material	Specific surface area ($m^2\ g^{-1}$)	Pore diameter (nm)	Pore volume ($cm^3\ g^{-1}$)
SBA-15	623	6.5	1.23
NH_2-SBA-15	485	5.8	0.67
TS-SBA-15	396	5.5	0.41

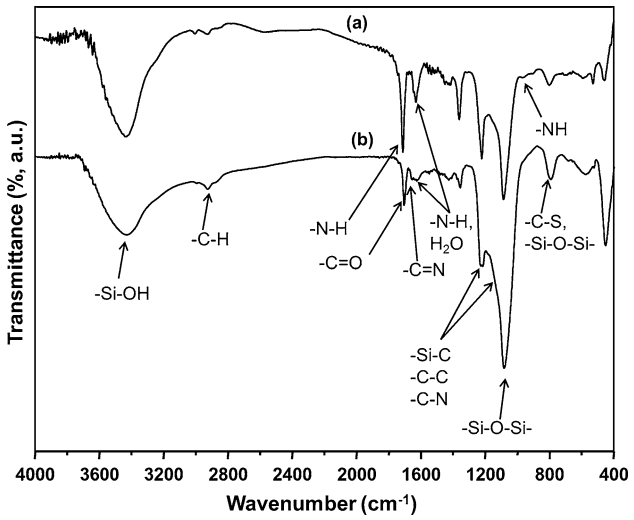

Fig. 2 FTIR spectra of (*a*) NH_2-SBA-15 and (*b*) TS-SBA-15

surface of SBA-15. In addition, the characteristic band for the aliphatic –C–H stretching vibrations was observed due to the pendant alkyl chains at approximately 3000–2800 cm^{-1} [36]. The strong peaks at 1084 and 795 cm^{-1} were assigned to the asymmetric stretching vibration of Si–O–Si present in the framework of the SBA-15 [37]. The peak at ca. 1630 cm^{-1} might be due to the –OH bending vibration from adsorbed water. In addition, the stretching vibration of ethoxy groups was observed at 2999 cm^{-1}. This can be explained by the interaction of APTES with the isolated silanol groups, where not all ethoxy groups were condensed to the silica matrix. Furthermore, the IR spectra strongly support the presence of absorption bands due to N–H bonds (1713, 1645 and 3400 cm^{-1}), while the relatively broad peaks at 780 and 1160 cm^{-1} indicate the presence of an N–H wagging vibration in the NH_2-SBA-15 material [37]. The bending vibration of primary amine groups $–NH_2$ can be observed between 1650 and 1580 cm^{-1}, which could only be visible in a primary amine compound. In addition, this band is considered the vibrational band of the protonated form of amino groups, e.g. $–NH_3^+$, which could be formed due to the presence of adsorbed water or neighbouring silanol groups. The absorbance of the C–N stretching vibration is normally observed at 1000–1200 cm^{-1}. On the other hand, this peak was not observed because of its overlap with the absorbance of the Si–O–Si and $Si–CH_2$ stretch in the 1000–1300 cm^{-1} range. The TS-SBA-15 displayed a strong band near 1650 and 794 cm^{-1} due to azomethine (C=N) and thiophene ring C–S stretching vibrations, respectively [38]. Additionally, the presence of a peak at 1704 cm^{-1} in TS-SBA-15 sample indicates the –C=O stretching vibration of the unattached MTC molecule in the pore channels [39]. The above FTIR bands confirmed the successful anchoring of APTES and subsequent tailoring to the MTC Schiff base on the SBA-15 surface.

3.5 Solid-state ^{29}Si MAS and ^{13}C CP-MAS NMR analyses

Information on the silicon environment and the degree of functionality was obtained from the ^{29}Si MAS NMR spectra (Fig. 3) of (a) SBA-15 and (b) NH_2-SBA-15. In the spectrum of SBA-15, the signals due to $SiO_2(OH)_2$ (Q^2 sites) at −92 ppm, SiO_3–OH (Q^3 sites) at −100 ppm and SiO_4 (Q^4 sites) at −109 ppm were observed. Prior to functionalisation, the most intense peak was Q^3 (at ca. −100 ppm), which suggests that the predominant silicon species are $(SiO)_3Si–OH$, as expected from a SBA-15-type material [40]. This confirmed the formation of a perfect porous material with a highly cross-linked silica framework and the presence of sufficient surface silanol groups for functionalising the material. After functionalisation with propylamine over SBA-15, the intensity of the Q^3 peak decreased and the intensity of Q^4 increased. In addition, three additional broad and overlapping signals appeared at $\delta \approx -59$ and −66 ppm, which were assigned to T^2 and T^3 organosilica species, respectively, with T^3 as the major peak [40, 41]. The ^{13}C CP-MAS NMR spectra of (a) NH_2-SBA-15 and (b) TS-SBA-15 (Fig. 4) showed the successful functionalisation of aminopropyl and subsequent formation of MTC Schiff base in the SBA-15 material. NH_2-SBA-15 showed three sharp peaks at 9.8 (C1), 27.1 (C2) and 44.6 (C3) ppm corresponding to methylene groups in the propyl chain [40, 41]. The additional less intense peaks in the spectrum were attributed to the presence of uncondensed ethoxy groups in the functionalised molecule, which was clearly observed by the presence of T^2 sites in the ^{29}Si MAS NMR spectrum of NH_2-SBA-15. TS-SBA-15 also revealed the resonances corresponding to the propyl carbon atoms in shifted positions, which were 10.2, 23.9 and 50.2 ppm for C1, C2 and C3, respectively. Additional resonances were observed in the spectrum of TS-SBA-15 at 10.1, 63.1, 153.5, 129.1, 124.4, and 142.5 ppm for C4, C5, C6, C7, C8, and C9, respectively [34, 42].

3.6 Thermogravimetric analysis

The TGA curves of (a) NH_2-SBA-15 and (b) TS-SBA-15 (Fig. S4) revealed 1 and 2 % weight losses, respectively, at temperatures up to ca. 120 °C, which were attributed to the desorption of physically adsorbed water. The decomposition of NH_2-SBA-15 and TS-SBA-15 began slowly from 150 °C, followed by a sudden weight loss between 230 and 600 °C is due to the combustion of 5-methyl-2-thiophenecarboxaldehyde Schiff base present in the material

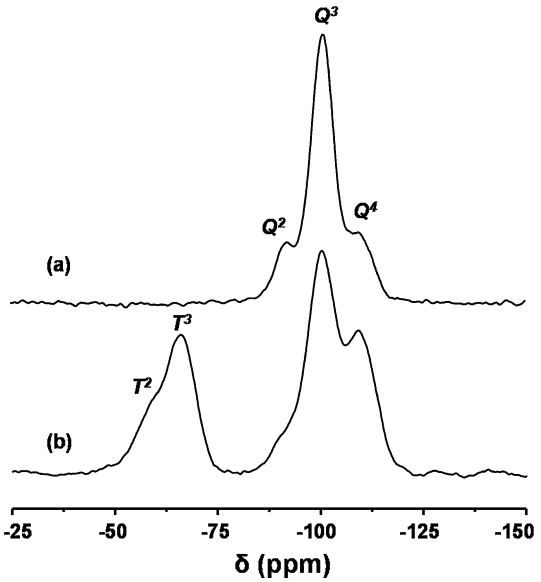

Fig. 3 ^{29}Si MAS NMR spectra of (*a*) SBA-15 and (*b*) NH_2-SBA-15

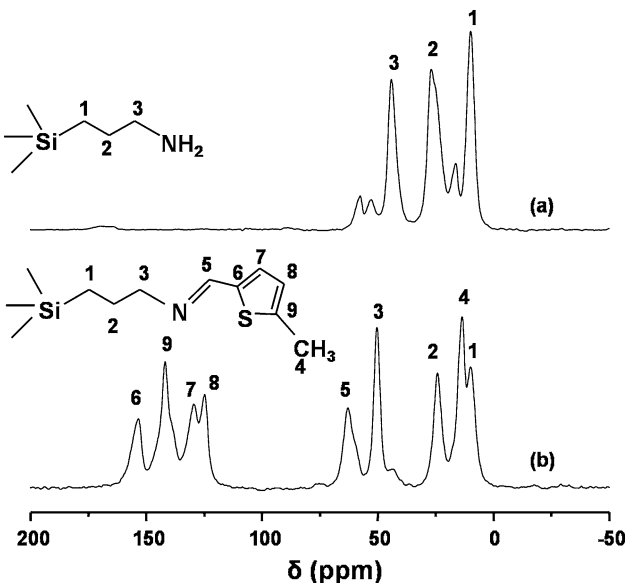

Fig. 4 ^{13}C CP-MAS NMR spectra of (*a*) NH_2-SBA-15 and (*b*) TS-SBA-15

[40, 43, 44]. The total weight loss in this region was 16 and 29 wt% for NH_2-SBA-15 and TS-SBA-15, respectively. The amount of MTC Schiff base was calculated to 1.47 mmol g^{-1} considering the molecular weight of functionalised molecule after losing the ethanol molecules during the immobilisation process. The degradation process was completed at 700 °C and the rather extended temperature range was caused by several chemical reactions, such as oxidation reactions, "channel metamorphosis" via proton transfer from silanols to methylene groups and also due to an increase in the number of siloxane bridges (Si–O–Si) caused by isolated silanol condensation [34, 45].

3.7 Adsorption of metal ions from aqueous solutions using TS-SBA-15

3.7.1 Adsorption selectivity of metal ions from a multimetal ion mixture

Before selecting the metal ions for the adsorption study, competitive adsorption from a mixture containing 1 mM each of Mn(II), Co(II), Ni(II), Cr(III), Zn(II), Pb(II) and Cd(II) ions at pH 6 was conducted. TS-SBA-15 (0.01 g) was added to 10 ml of the above solution and shaken for 24 h to establish the adsorption equilibrium. The experiment was conducted to determine the suitable metal ions for the adsorption study. Figure 5 shows the weight and mole adsorption selectivity of the metal ions after adsorption from the above mixture using TS-SBA-15. TS-SBA-15 is more selective towards Cr(III), Pb(II) and Zn(II) under the specified experimental conditions. The mole adsorption selectivity was in the order of Cr(III) > Pb(II) > Zn(II).

3.7.2 Adsorption of Cr(III), Pb(II) and Zn(II) from single metal ion solutions

Adsorption processes are normally considered intermolecular interactions among the solute and solid phases. In the case of organic molecule-immobilised porous materials, the adsorption of metal ions from solution is an interaction of the solute molecule with the surface functionality by electrostatic, hydrogen bonding, weak Van der Waals force of attraction or even complexation. All mechanisms depend greatly on the pH, contact time, initial ionic strength, and adsorbent dosage. Therefore, it is important to determine the effects of such factors on the adsorption nature and mechanism during the adsorption process.

The initial solution pH is an important factor affecting the adsorption of heavy metal ions; because it not only influences the surface charge of the adsorbents, but also the type of metal ions in solution. Therefore, a study was conducted to optimise the pH with the other parameters, such as the TS-SBA-15 dose, metal ion concentration and contact time, kept constant. The effects of pH on the adsorption of Cr(III), Pb(II) and Zn(II) from water samples was studied over the pH range, 3–6.5, for initial concentrations of 1 mM onto TS-SBA-15, as illustrated in Fig. 6a. Higher pH values were not studied due to the precipitation limitation of metal ions and the instability of functionalised mesoporous silicates in alkali solutions. All three metal ions exhibited similar adsorption behaviour over the entire pH range. As shown in the figure, the adsorption capacity was increased considerably when the pH was increased

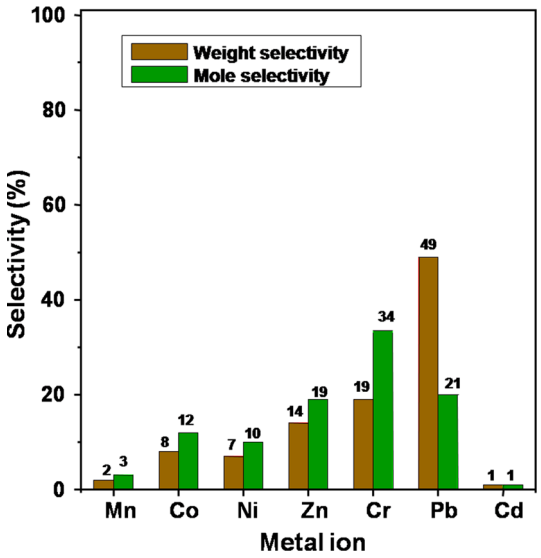

Fig. 5 Adsorption selectivities of TS-SBA-15 from a mixture containing Mn(II), Co(II), Ni(II), Zn(II), Cr(III), Pb(II) and Cd(II) ions. Adsorption conditions—initial concentration: 1.0 mM (each metal ions), volume of metal solution: 10.0 ml, amount of adsorbent: 0.01 g, time 24 h, pH 6, and temperature: RT

from 3.0 to 6.5 [34, 46]. This can be explained by the protonation effect of H^+ ions present at higher concentrations in solution on the N and S atoms of the MTC Schiff base adsorbent. At very low solution pH, the concentration of H^+ ions in adsorption medium is very high, which was competing directly with the heavy metal ions for active binding sites [47, 48]. Additionally, due to the smaller size of the H^+ than metal ions, it can approach the ligand atoms very easily. As a result, the adsorption of metal ions will decrease with respect to an increase of the acidic strength in the solution. At higher pH, the surface of the adsorbent had a higher negative charge, resulting in higher attraction towards the cations. As an explanation, TS-SBA-15 adsorbed Cr(III), Pb(II) and Zn(II) ions from the aqueous solutions with a maximum of 31, 82 and 22 mg g^{-1} at pH 6.5. In addition, the maximum number of active sites was estimated to be 1.47 mmol g^{-1}, and the maximum adsorption of Cr(III), Pb(II) and Zn(II) ions was 0.60, 0.40 and 0.34 mmol g^{-1}. This suggests that the adsorption follows a mechanism corresponding to Scheme S1. At very high pH, metal hydroxides are formed, which resulted in precipitation; therefore, the separation may not have been achieved due to adsorption. When the pH was increased from 3 to 6.5, the removal efficiency of TS-SBA-15 for Cr(III), Pb(II) and Zn(II) was increased from 35 to 60, 20 to 40 and 12 to 34 %, respectively. To explain this observation, at pH < 7, all the metal ions in solution exist as M^{n+} and $M(OH)^+$. Therefore, most ions are accessible to the adsorbent at a pH near to neutral condition, resulting in an increase in removal efficiency [34, 49].

To determine the suitable contact time for the maximum removal efficiency of TS-SBA-15, the equilibrium contact time was examined. A 0.01-g sample of TS-SBA-15 was suspended in a Cr(III)/Pb(II)/Zn(II) solution (10 ml, 1 mM) and the mixture was stirred mechanically at 25 °C for times, ranging from 0.25 to 24 h at pH 6.5. Subsequently, the mixture was filtered, and the concentration of heavy metal ions remaining in solution was determined by ICP-AES. Plots of the amount of adsorption versus stirring time (Fig. 6b) suggested that the adsorption of all metal ions increased with time. All three metal ions showed adsorption equilibrium within 6 h. The reasonably fast kinetics of the matrix–metal ions interaction reflects the good accessibility of the chelating sites of the modified matrix and high binding ability of the metal ions [26, 34].

The metal ion removal efficiency by a mesoporous material depends greatly on the bonding strategy between the metal ion and the donor atoms of the anchored molecule on the surface. In addition, the adsorption equilibrium can be altered in the adsorbent or adsorbate by merely altering the concentration of metal ions. To examine the effects of the initial metal ion concentration, a 0.01-g sample of TS-SBA-15 was suspended in 10 ml of Cr(III)/Pb(II)/Zn(II) solution with a concentration in the range, 1–5 mM, at pH 6.5. The mixture was stirred mechanically at 25 °C for 6 h. The mixture was filtered, and the concentration of heavy metal ions remaining in solution was determined by ICP-AES. Figure 6c shows the amount of Cr(III)/Zn(II)/Pb(II) ion adsorption as a function of the initial metal ion concentration in solution. The change in the initial metal ion concentration had a significant effect on the removal efficiency [50, 51]. At low metal ion concentrations, the ratio of surface active sites to the total metal ions in the solution was high; hence, a major portion of the metal ions in solution may interact with the adsorbent and be removed from solution. At higher initial metal ion concentrations, there was a slight increase in the amount of adsorption. On the other hand, the rate of the increase in adsorption was reduced at very high initial concentrations. In contrast, TS-SBA-15 could adsorb a maximum of 0.71, 0.62 and 0.50 mmol g^{-1} Cr(III), Pb(II) and Zn(II) ions, respectively, from aqueous solutions with an initial metal ion concentration of 5 mM. The slower rate of increase in adsorption is the result of the adsorption/desorption equilibrium achieved between metal ions in solution and the adsorbent [28, 34]. The maximum amount of all metal ions adsorbed from a 5 mM solution also strongly supports the adsorption mechanism corresponding to Scheme S1.

Figure 6d shows the effects of the adsorbent dosage on the adsorption efficiency of Cr(III), Pb(II) and Pb(II) onto TS-SBA-15 at pH 6.5. 0.01, 0.02, 0.03, 0.04 and 0.05 g of adsorbent were selected for the uptake of Cr(III), Pb(II) and

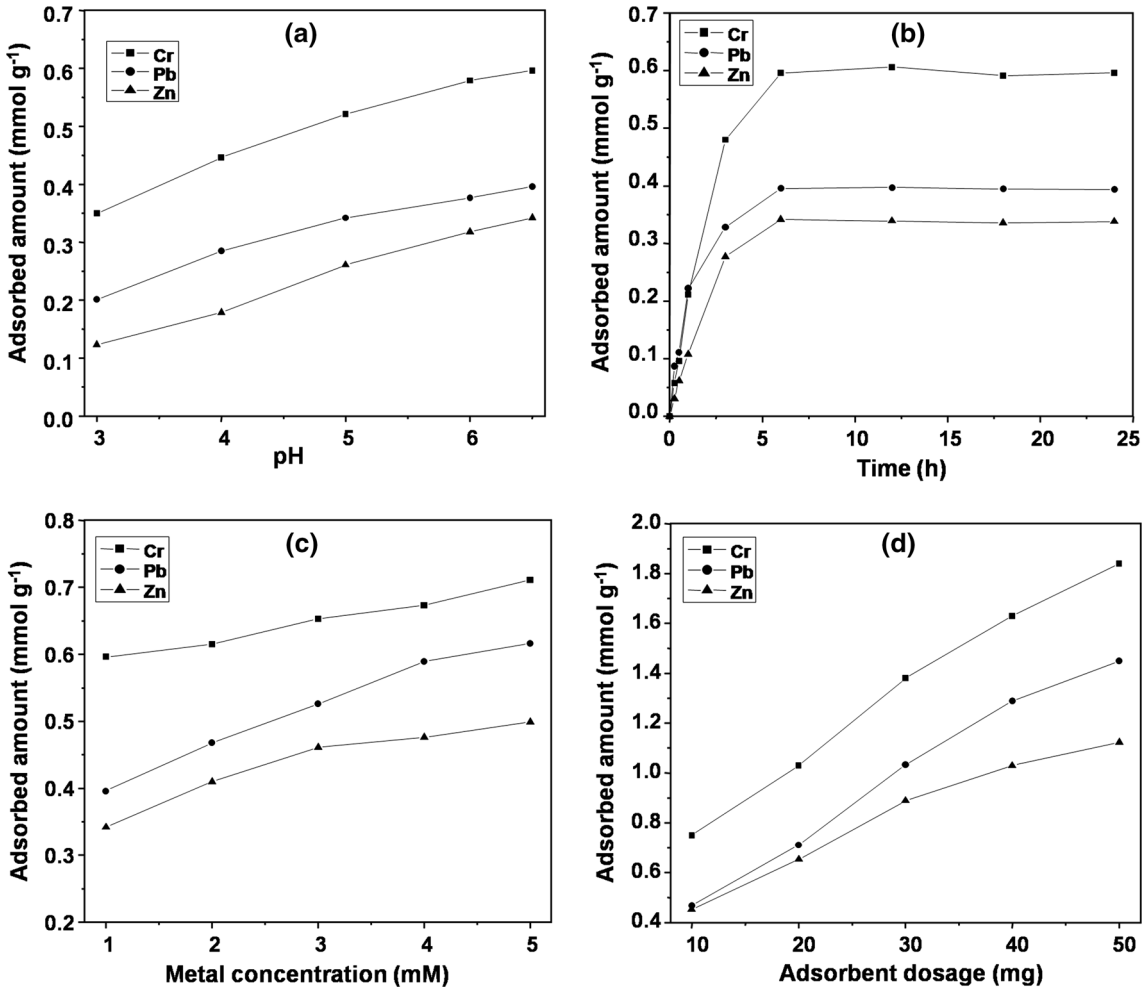

Fig. 6 Effect of various factors on Cr(III), Pb(II) and Zn(II) adsorption; **a** pH of the metal solution (concentration: 1.0 mM, adsorbate volume: 10 ml, adsorbent dosage: 0.01 g, time: 24 h), **b** stirring time (concentration: 1 mmol, adsorbate volume: 10.0 ml, adsorbent dosage: 0.01 g, pH: 6.5), **c** initial metal ion concentration (adsorbate volume: 10.0 ml, adsorbent dosage: 0.01 g, pH: 6.5, time: 6 h) and **d** adsorbent dosage (concentration: 2.0 mM, adsorbate volume: 10.0 ml, pH: 6.5, time: 6 h)

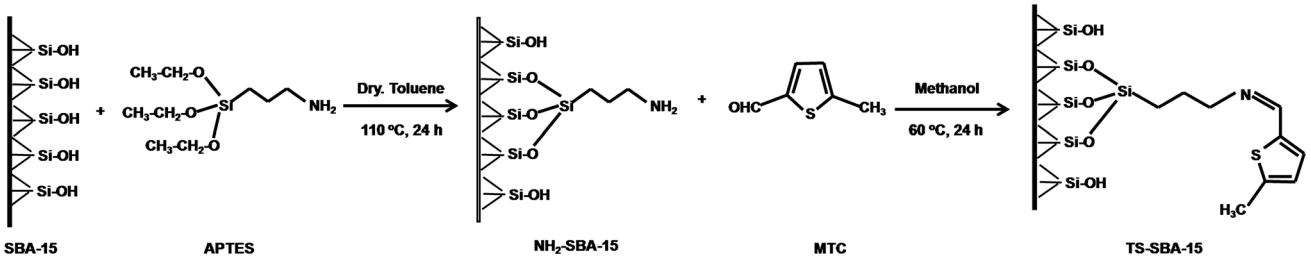

Scheme 1 Synthesis of 5-methyl-2-thiophenecarboxaldehyde Schiff base-immobilized SBA-15

Zn(II) from an initial metal ion solution of 2 mM. The percentage removal was increased from 30 to 92, 23 to 72 and 20 to 56 % for Cr(III), Pb(II) and Zn(II), respectively, when the adsorbent dosage was increased from 0.01 to 0.05 g. A higher adsorbent dose indicates more active functional groups for the uptake of metal ions onto the TS-SBA-15 surface, which results in a high removal percentage. The maximum removal of 92 % was achieved for Cr(III) at a dose of 0.05 g TS-SBA-15. The maximum removal of 1.84, 1.45 and 1.12 mmol g^{-1} were achieved for Cr(III), Pb(II) and Zn(II), respectively, when 0.05 g of adsorbent was used. These results also showed that the metal removal percentage is strongly dependent on the optimal increase in adsorbent dose, due to a consequential

increase in interference between the binding sites at the higher dose or an insufficiency of metal ions in solution with respect to the available binding sites [15, 52].

3.7.3 *Adsorption selectivity of metal ions from binary and ternary mixtures*

Finally, the selective affinity of TS-SBA-15 for metal ion adsorption from binary and ternary mixtures of Cr(III), Pb(II) and Zn(II) ions was investigated. The competitive adsorption of coexisting ions to the binding sites is normally a severe problem when using adsorbents with organic functional groups as the active sites for the removal of heavy metals. Figure 7 shows the weight and mole adsorption selectivities of binary solutions of (a) Cr(III) and Pb(II), (b) Cr(III) and Zn(II) and (c) Pb(II) and Zn(II). Binary metal ion mixtures containing nitrate salts of Cr(III), Zn(II) and Pb(II) with 1 mM concentration of each metal ion in water were prepared. A total of 10 ml of the above solution was mixed with 0.01 g of the TS-SBA-15 and shaken for 6 h to achieve the adsorption equilibrium. The competitive adsorption from the binary mixtures (a) and (b) revealed the higher affinity of TS-SBA-15 towards Cr(III) ions. The mole adsorption selectivities of Cr(III) in these mixtures are 65 and 72 % (Fig. 7a, b), respectively. Also TS-SBA-15 exhibited (Fig. 7c) a higher affinity towards Pb(II) ion (69 %), when considering the mole adsorption selectivities of the component metal ions in the binary mixture of Pb(II) and Zn(II). The adsorption selectivity of Zn(II) ion was slightly higher when the adsorption occurred in a mixture with Pb(II) than Cr(III). The adsorption from binary mixtures revealed the superior adsorption selectivity of Cr(III) ions, suggesting the strong binding ability of Cr(III) ions with the chelating bidentate ligand [34].

In order to find out the effect of the increased concentration of Pb(II)/Zn(II) over the selectivity of Cr(III) adsorption from binary mixtures, we have conducted the selective adsorption from Cr/Zn with 1:2 and 1:5 mM concentrations and Cr/Pb with 1:2 mM concentration. TS-SBA-15 exhibited a mole and weight selectivities for Zn(II) of 28 and 33 % (Fig. 7b), respectively, when the adsorption occurs from the binary mixture of Cr/Zn with 1:1 mM concentration. When increasing the concentration of Zn(II) from 1.0 (Fig. 7b) to 2.0 mM (Fig. 8a) in Cr/Zn mixture, a nominal increase in mole selectivity of 31 % was observed. But an increase of Zn(II) concentration from 1.0 (Fig. 7b) to 5.0 (Fig. 8b) mM in Cr/Zn mixture triggered a mole selectivity increase in Zn(II) from 28 (Fig. 7b) to 46 % (Fig. 8b). Interestingly, when increasing the concentration of Pb(II) from 1.0 (Fig. 7a) to 2.0 mM (Fig. 8c) in Cr/Pb mixture, both mole and weight selectivities were markedly increased from 35 and 68 % (Fig. 7a) to 63 and 87 % (Fig. 8c), respectively. This experiment confirmed the marked effect of concentration on the metal adsorption selectivity of TS-SBA-15 from aqueous mixture.

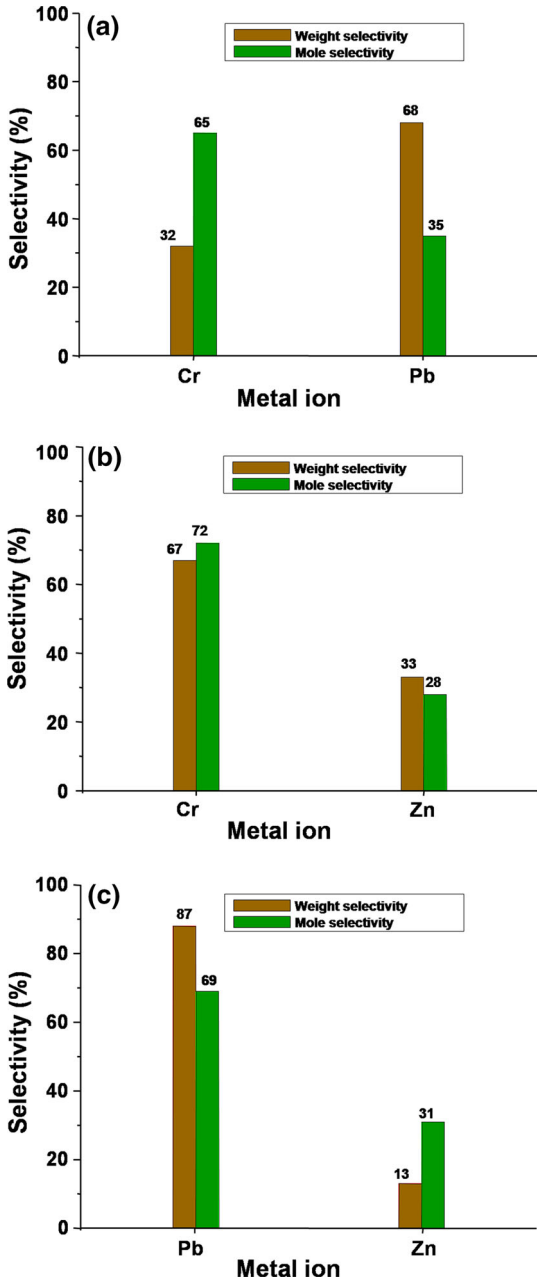

Fig. 7 Adsorption selectivities of TS-SBA-15 from binary mixtures of **a** Cr/Pb, **b** Cr/Zn and **c** Pb/Zn with 1:1 mM concentration. Adsorption conditions—volume of metal solution: 10.0 ml, amount of adsorbent: 0.01 g, time: 6 h, pH 6.5, and temperature: RT

Figure 9 presents the adsorption selectivity profiles of TS-SBA-15 in the ternary metal ion solution with respect to the combination in concentration of component ions. To examine the effects of concentration on the adsorption selectivity, the concentration of at least one component in

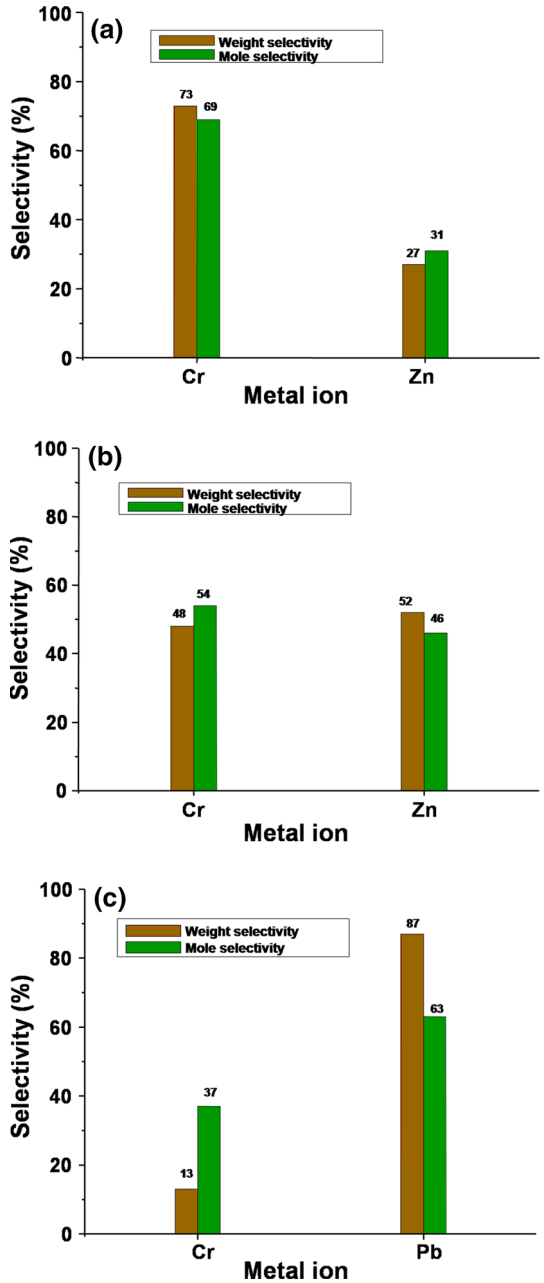

Fig. 8 Adsorption selectivities of TS-SBA-15 from binary mixtures of **a** Cr/Zn, **b** Cr/Zn and **c** Cr/Pb with 1:2, 1:5 and 1:2 mM concentrations, respectively. Adsorption conditions—volume of metal solution: 10 ml, amount of adsorbent: 0.01 g, time: 6 h, pH 6.5, and temperature: RT

the mixture was doubled. The result was compared with the ternary solution containing equal concentrations of component metal ions. The behaviour of adsorption can be observed by analysing the mole selectivity of each metal ion after adsorption from each combination. The adsorption selectivity from a 1:1:1 (Cr/Pb/Zn) combination showed that TS-SBA-15 was adsorbed 63, 35 and 2 mol% of Cr, Pb and Zn ions, respectively (Fig. 9a). In addition, the mole selectivity of Zn(II) ion was increased to 6 % (Fig. 9b) when the concentration of Zn(II) in the ternary solution (1:1:2) was doubled. Interestingly, Zn(II) did not show any adsorption from the 2:1:1 and 1:2:1 mixtures. The mole selectivity of Cr(III) and Pb(II) increased from 63 to 91 and 35 to 47 mol%, respectively, when their concentrations were doubled (Fig. 9c, d). Every combination exhibited dominant adsorption selectivity to the Cr(III) ion. These results strongly support the higher binding ability of Cr(III) with TS-SBA-15 than Pb(II) and Zn(II). In addition, the concentration, combination and number of component ions in a mixture have a solid effect on the adsorption selectivity over the TS-SBA-15 adsorbent.

From the selectivity experiments, TS-SBA-15 was more selective for Cr(III) ions. The mole adsorption selectivity from aqueous mixtures will be always a factor of the nature of the ligand, chelation effect, ionic size, and ionic potential (charge to radius ratio) of metal ions. The complexation ability of the MTC Schiff base is due mainly to the chelation property of N and S donor atoms in such a molecule. A chelated complex will be always stable due to the significant gain in entropy. Moreover, thiophene bearing an electron-donating methyl group adjacent to the sulphur atom imparts a high electron density over the sulphur atom, which will increase the ligation efficiency of the ligand. As a result, the MTC Schiff base can adsorb metal ions more strongly and efficiently from solution, even though it will introduce a small amount of steric hindrance at the active site compared to the ligand without a methyl group, which was reported previously [25, 26]. The ionic potential of Cr(III), Zn(II) and Pb(II) ions are 4.83, 2.7 and 1.69, respectively. In addition, Cr(III) has a more positive charge, smaller ionic radius and greater ionic potential than the other two ions. As a result, Cr(III) can make a strong dative bond with the MTC Schiff base ligand more easily than Zn(II) and Pb(II). Therefore, TS-SBA-15 was found to be more active for Cr(III) from the metal ion mixture.

3.7.4 Reusability of TS-SBA-15

The effectiveness and stability of the sorbent were evaluated by a reusability test, which could be done by an acid, base or salt treatment with or without an organic stripping agent. A series of sorption/desorption experiments was performed under acid conditions to understand the adsorption efficiency in multiple regeneration. Figure 10 presents the Cr(III)/Pb(II)/Zn(II) adsorption efficiency of TS-SBA-15 after six recycle steps. After sorption, the sorbent was treated with a mixture containing NHO_3 and thiourea with 1.0 mol l^{-1} individual concentration to desorb Cr(III)/Pb(II)/Zn(II), and this sorption/desorption procedure was repeated six times [52]. After each desorption

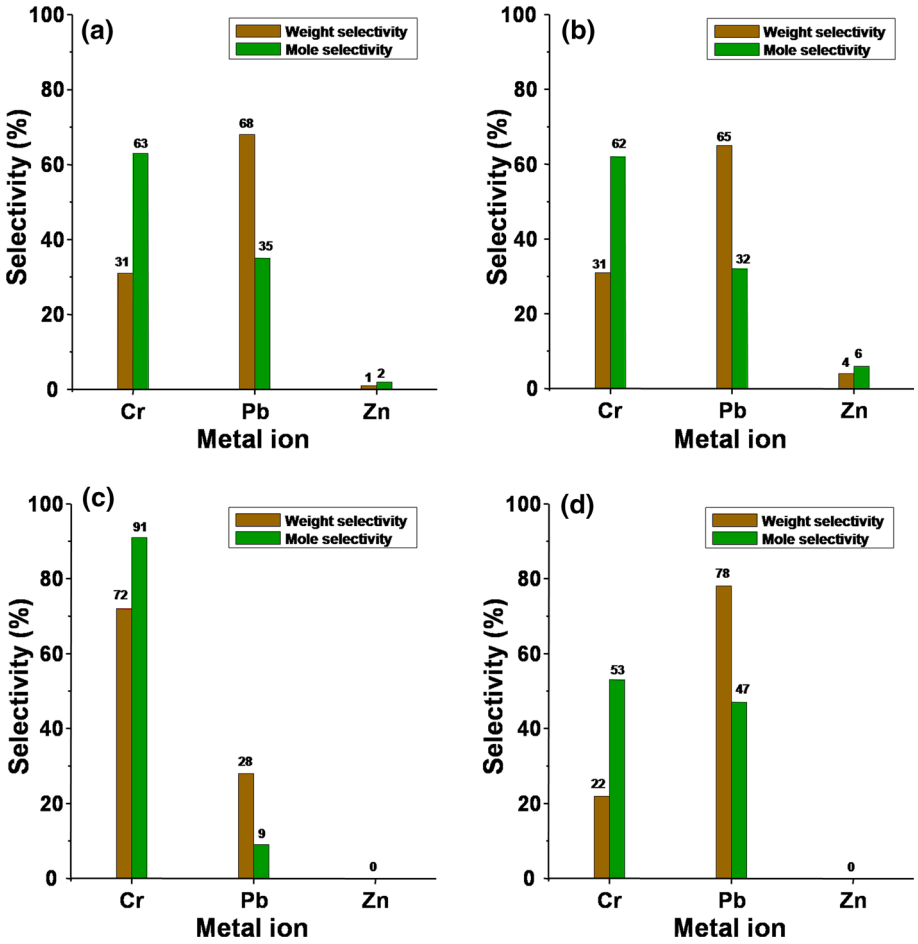

Fig. 9 Adsorption selectivities of TS-SBA-15 from the ternary mixture, Cr/Pb/Zn with **a** 1:1:1, **b** 1:1:2, **c** 2:1:1, and **d** 1:2:1 mM concentrations. Adsorption conditions—volume of metal solution: 10.0 ml, amount of adsorbent: 0.01 g, time: 6 h, pH 6.5, and temperature: RT

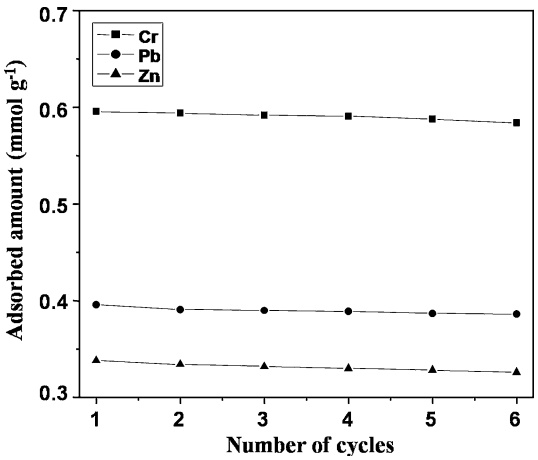

Fig. 10 Adsorption cycles of Cr(III), Pb(II) and Zn(II) on TS-SBA-15. Adsorption condition—pH of the metal solution: 6.5, concentration of metal solution: 1.0 mM, adsorbate volume: 10.0 ml, adsorbent dosage: 0.01 g, time: 6 h

step, the sorbent was washed with doubly distilled water to remove the metal salt and thiourea generated from the pore channels. A negligible decrease in sorption capacity was observed after six consecutive uses of 0.05 g of TS-SBA-15.

3.7.5 Equilibrium study

The adsorption isotherm models are normally used to describe the interaction between adsorbents and adsorbates, providing most important parameters for designing a desired adsorption system. Therefore, the Cr(III), Pb(II) and Zn(II) removal capacity of the TS-SBA-15 was determined, where the Langmuir and Freundlich adsorption models were applied to evaluate the effectiveness of the adsorbent [53].

The Langmuir model is based on the assumption that the maximum adsorption occurs when a saturated monolayer of solute molecules is present on the adsorbent surface, the energy of adsorption is constant and there is no migration of adsorbate molecules in the surface plane. Figures S5a, S6a and S7a show the experimental result of the Langmuir isotherms of Cr(III), Pb(II) and Zn(II) adsorption, respectively, on TS-SBA-15.

According to the Langmuir isotherm,

$$q_e = \frac{q_m K_L C_e}{1 + K_L C_e}$$

The constants in the Langmuir isotherm can be determined by plotting C_e versus C_e/q_e and making use of the above rewritten as:

$$\frac{C_e}{q_e} = \frac{1}{K_L q_m} + \frac{C_e}{q_m}$$

where q_m and K_L are the Langmuir constants, representing the maximum adsorption capacity for the solid-phase loading and the energy constant related to the heat of adsorption, respectively.

The Freundlich isotherm model is an empirical relationship describing the adsorption of solutes from a liquid to a solid surface and assumes that different sites with several adsorption energies are involved. The Freundlich adsorption isotherm is the relationship between the amounts of Cr(III), Pb(III) and Zn(III) adsorbed per unit mass of adsorbent, q_e, and the concentrations of the Cr(III), Pb(II) and Zn(II) at equilibrium, C_e, as shown in Fig. S5b, S6b and S7b, respectively.

$$q_e = K_f C_e^{1/n}$$

The logarithmic form of the equation becomes

$$\ln q_e = \ln K_f + \frac{1}{n} \ln C_e$$

where K_f and n are the Freundlich constants, the characteristics of the system. K_f and n are the indicators of the adsorption capacity and adsorption intensity, respectively. The ability of the Freundlich model to fit the experimental data was examined. In this case, a plot of ln C_e versus ln q_e was used to generate the intercept of K_f and the slope of n.

Table S1 lists the values of the parameters for the Langmuir and Freundlich isotherm models. The R^2 values of Cr(III), Pb(II) and Zn(II) adsorption were 0.998, 0.995 and 0.999, respectively. The values of q_m and K_L of Cr(III) adsorption over TS-SBA-15 were 37 mg g^{-1} and 0.026 L mg^{-1}, respectively at pH 6.5 [54]. Also the q_m values of 127 and 32 mg g^{-1} and K_L values of 0.002 and 0.027 L mg^{-1}, respectively, for Pb(II) and Zn(II) ions. The Freundlich constants K_f for Cr(III), Pb(II) and Zn(II) adsorption were 0.070, 0.223 and 0.210 mg L g^{-1}, respectively. It was also noticed that the R^2 values of Cr(III), Pb(II) and Zn(II) adsorption were 0.920, 0.993 and 0.994, respectively. The R^2 value of Freundlich isotherm was found to be lower than the same of Langmuir isotherm. As a result, the adsorption mechanism is more fit into the Langmuir than Freundlich model. The magnitudes of K_f and n show the easy separation of all the three metal ions from the aqueous solution and favourable adsorption. The intercept K_f is an indication of the adsorption capacity of the adsorbent; the slope $1/n$ indicates the effect of concentration on the adsorption capacity and represents the adsorption intensity. As shown above, the n value was found to be high enough for separation. In addition, TS-SBA-15 gives the adsorption energy for adsorbing Cr(III), Pb(II) and Zn(II). The Langmuir isotherm fitted very well with a high correlation coefficient for all the metal ions, showing that the adsorption followed the Langmuir model [55, 56].

4 Conclusions

Covalently functionalised MTC Schiff base onto the SBA-15 surface was achieved successfully using a two-step post-synthetic grafting method. The physico-chemical properties of SBA-15, NH_2-SBA-15 and TS-SBA-15 were explored using a range of spectroscopic techniques. The formation of the uniform and ordered mesoporous materials was confirmed by SAXS, N_2-isotherm and TEM. The surface area, pore diameter and pore volume decreased, whereas the organic functionality inside the SBA-15 material increased. ^{29}Si MAS NMR provided a clear picture regarding the changing silica atmosphere in the support material with modification. ^{13}C CP-MAS NMR spectroscopy revealed the unambiguity in the anchoring of the (3-aminopropyl)triethoxysilane and 5-methyl-2-thiophenecarboxaldehyde over SBA-15. FTIR spectroscopy further supported the NMR results. The mesoporous SBA-15-supported MTC Schiff base ligand was used for the adsorption of Cr(III), Zn(II) and Pb(II) from aqueous solutions. The hydrophilic and bidentate characteristics of the functional organic moiety over SBA-15 rendered the modified mesoporous material useful for adsorption applications. The experiments showed that the best pH is 6.5 and time of adsorption for achieving the maximum level of adsorption was 6 h. In addition, TS-SBA-15 was highly active for the effective adsorption of metal ions under consideration. The selectivity study from binary and ternary mixtures showed that the ligand was selective in the order of Cr(III) > Pb(II) > Zn(II). In addition, the selectivity scenario is strongly dependent on the concentration of the component metal ions in a mixture. The regeneration studies showed that the TS-SBA-15 adsorbent synthesised in this study exhibited good regeneration efficiency up to six cycles.

Acknowledgments The authors thank to the National Research Foundation of Korea through the Ministry of Science, ICT & Future Planning, Korea; Pioneer Research Center Program (2010-0019308/2010-0019482); Acceleration Research Program (2014R1A2A1110054584); Brain Korea 21 Plus Program (21A2013800002) for financial support.

References

1. Kresge CT, Leonowicz ME, Roth WJ, Vartuli JC, Beck JS (1992) Nature 359:710–712
2. Corma A (1997) Chem Rev 97:2373–2420
3. Serna-Guerrero R, Sayari A (2007) Environ Sci Technol 41:4761–4766
4. Guliants VV, Carreon MA, Lin YS (2004) J Membr Sci 235:27–53
5. Yang H, Coombs N, Sokolova I, Ozin GA (1997) J Mater Chem 7:1285–1290
6. Zhao D, Feng J, Huo Q, Melosh N, Fredrickson GH, Chmelka BF, Stucky GD (1998) Science 279:548–552
7. Sujandi LO, Park SE, Han DS, Han SC, Jin MJ, Ohsuna T (2006) Chem Commun 39:4131–4133
8. Karvelas M, Katsoyiannis A, Samara C (2003) Chemosphere 53:1201–1210
9. Koehler FM, Rossier M, Waelle M, Athanassiou EK, Limbach LK, Grass RN, Gunther D, Stark WJ (2009) Chem Commun 32:4862–4864
10. Khan MM, Nair AS, Babu VJ, Murugana R, Ramakrishna S (2012) Energy Environ Sci 5:8075–8109
11. Florence TM, Batley GE (1976) Talanta 23:179–186
12. Griffith CS, Luca V, Cochrane J, Hanna JV (2008) Microporous Microporous Mater 111:387–403
13. Hossain KZ, Mercier L (2002) Adv Mater 14:1053–1056
14. Kim Y, Kim C, Choi I, Rengaraj S, Yi J (2004) Environ Sci Technol 38:924–931
15. Awual MR, Rahman IMM, Yaita T, Khaleque MA, Ferdows M (2014) Chem Eng J 236:100–109
16. Shiri-Yekta Z, Yaftian MR, Nilchi A (2013) Korean J Chem Eng 30:1644–1651
17. Singh UG, Williams RT, Hallam KR, Allen GC (2005) J Solid State Chem 178:3405–3413
18. Sutra P, Brunel D (1996) Chem Commun 21:2485–2486
19. Wang J, Lv M, Wang Z, Zhou M, Gu C, Guo C (2015) J Photochem Photobiol, A 309:37–46
20. Wang Q, Gao W, Liu Y, Yuan J, Xu Z, Zeng Q, Li Y, Schröder M (2014) Chem Eng J 250:55–65
21. Hoffmann F, Cornelius M, Morell J, Froeba M (2006) Angew Chem Int Ed 45:3216–3251
22. Huang X, Liao X, Shi B (2010) J Hazard Mater 173:33–39
23. Jorgetto Ade O, Pereira SP, Silva RI, Saeki MJ, Martines MA, Pedrosa Vde A, Castro GR (2015) Acta Chem Slov 62:111–121
24. Wua XW, Maa HW, Yanga J, Wang FJ, Li ZH (2012) Appl Surf Sci 258:5516–5521
25. Soliman EM, Saleh MB, Ahmed SA (2004) Anal Chim Acta 523:133–140
26. Jamalia MR, Assadi Y, Shemirani F, Niasari MS (2007) Talanta 71:1524–1529
27. Parambadath S, Singh AP (2009) Catal Today 141:161–167
28. Shahbazi A, Younesi H, Badiei A (2011) Chem Eng J 168:505–518
29. Chen SY, Huang CY, Yokoi T, Tang CY, Huang SJ, Lee JJ, Chan JCC, Tatsumi T, Cheng S (2012) J Mater Chem 22:2233–2243
30. Lombardo MV, Videla M, Calvo A, Requejo FG, Soler-Illia GJAA (2012) J Hazard Mater 223–224:53–62
31. Hsu YC, Hsu YT, Hsu HY, Yang CM (2007) Chem Mater 19:1120–1126
32. Acuña RH, Nava R, Peza-Ledesma CL, Lara-Romero J, Alonso-Núñez G, Pawelec B, Rivera-Muñoz EM (2013) Materials 6:4139–4167
33. Du G, Lim S, Pinault M, Wang C, Fang F, Pfefferle L, Haller GL (2008) J Catal 253:74–90
34. Mathew A, Parambadath S, Kim SY, Park SS, Ha CS (2015) J Porous Mater 22:831–842
35. Dindar MH, Yaftian MR, Rostamnia S (2015) J Environ Chem Eng 3:986–995
36. Moorthy MS, Park SS, Selvaraj M, Ha CS (2014) J Nanosci Nanotechnol 14:8891–8897
37. Wahab MA, Kim IL, Ha CS (2004) J Solid State Chem 177:3439–3447
38. Bardajee GR, Hooshyar Z, Shahidi FE (2015) Int J Environ Sci Technol 12:1737–1748
39. Radu GL, Truică GI, Penu R, Moroeanu V, Litescu SC (2012) UPB Sci Bull Ser B 74:137–148
40. Mathew A, Parambadath S, Park SS, Ha CS (2014) Microporous Microporous Mater 200:124–131
41. Perez Y, del Hierro I, Zazo L, Galan RF, Fajardo M (2015) Dalton Trans 44:4088–4101
42. Parambadath S, Mathew A, Barnabas MJ, Ha CS (2015) Microporous Microporous Mater 215:67–75
43. Luo Y, Lin J (2005) Microporous Microporous Mater 86:23–30
44. Guo W, Chen R, Liu Y, Meng M, Meng X, Hu Z, Song Z (2013) Colloid Surf A 436:693–703
45. Dong Z, Tian X, Chen Y, Hou J, Ma J (2013) RSC Adv 3:2227–2233
46. Gode F, Pehlivan E (2006) J Hazard Mater 136:330–337
47. Moazzen E, Daei N, Hosseini SM, Ebrahimzadeh H, Monfared A, Amini MM, Sadeghi O (2012) Microchim Acta 178:367–372
48. Ebrahimzadeh H, Tavassoli N, Sadeghi O, Amini MM, Vahidi S, Aghigh SM, Moazzen E (2012) Food Anal Methods 5:1070–1078
49. Qunaibit MA, Khalil M, Wassil AA (2005) Chemosphere 60:412–418
50. Bagheri A, Behbahani M, Amini MM, Sadeghi O, Taghizade M, Baghayi L, Salarian M (2012) Talanta 89:455–461
51. Bagheri A, Taghizadeh M, Behbahani M, Asgharinezhad AA, Salarian M, Dehghani A, Ebrahimzadeh H, Amini MM (2012) Talanta 99:132–139
52. Kumari V, Sasidharan M, Bhaumik A (2015) Dalton Trans 44:1924–1932
53. Zhao V, Sheng G, Hu J, Chen C, Wang X (2011) Chem Eng J 171:167–174
54. Park M, Choi CL, Seo YJ, Yeo SK, Choi J, Komarneni S, Lee JH (2007) Appl Clay Sci 37:143–148
55. Zhang F, Du N, Li H, Song S, Hou W (2015) Colloid Polym Sci 293:1961–1969
56. Ravi S, Selvaraj M (2014) Dalton Trans 43:5299–5308